Dalton Transactions

Accepted Manuscript

ROYAL SOCIETY OF CHEMISTRY

www.rsc.org/dalton

Table of contents entry

Novel 3D Au/$(BiO)_2CO_3$ heterostructures with size-controlled Au nanoparticles (2-10 nm) were first synthesized and applied in photocatalytic NO removal.

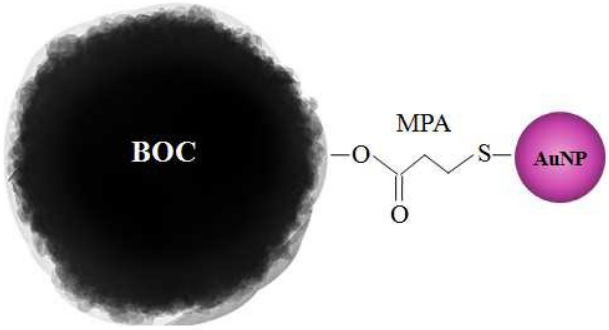

Dalton Transactions RSC Publishing

COMMUNICATION

Controlled Deposition of Au on $(BiO)_2CO_3$ Microspheres: Size and Content of Au Nanoparticles Matter †

Cite this: DOI: 10.1039/x0xx00000x

Received 00th January 2015,
Accepted 00th January 2015

DOI: 10.1039/x0xx00000x

www.rsc.org/

Qiuyan Li,‡[a] Xiaodong Hao,‡[b] Xiaolong Guo,[b] Fan Dong*[a] and Yuxin Zhang*[b,c]

Novel 3D Au/$(BiO)_2CO_3$ (Au/BOC) heterostructures with size-controlled Au nanoparticles (NPs) (2-10 nm) were first synthesized and applied in photocatalytic removal of ppb-level NO for air cleaning. The photocatalytic performance of Au/BOC heterostructures was enhanced by fine-tuning the contents of Au loading and the size of Au NPs. A new photocatalysis mechanism of surface scattering and reflecting (SSR) coupled with surface plasmon resonance (SPR) was proposed to understand the enhanced photocatalytic activity.

Introduction

In recent years, various types of semiconductor photocatalysts have been developed for environmental remediation and solar energy conversion. However, the high recombination rate of electron-hole pairs and low utilization of visible light result in a low photocatalytic activity.[1] Therefore, the development of photocatalysts with outstanding visible light activity is urgent and indispensable. The deposition of noble metal cocatalysts (Ag or Au) onto the surface of semiconductor has been demonstrated great potential for enhancing photocatalysis.[2-3] The noble metal NPs can facilitate the separation of charge carriers.[4-7] Also, the surface plasmon resonance (SPR) endowed by the noble metal NPs enables enhanced visible light absorption.[8-10]

The light absorption of the noble metal/semiconductor photocatalyst has been found to depend on the size of the noble metal NPs. When the particles grew bigger, the absorption band broadened and red-shifted to longer wavelengths.[11-12] Meanwhile, tuning the size of noble metal NPs could lead to changes of the surface areas and electronic structure, providing an opportunity to adjust the photocatalytic activity.[13] Zhang and co-workers reported that when Au particles with different sizes were deposited on the surface of zeolites, the photocatalytic activity of Au/zeolite in benzyl alcohol oxidation awas decreased with the increasing particle size.[14] For Au NPs on ZrO_2 photocatalyst, a significant decrease was also noted in the photocatalytic HCHO oxidation when the Au NPs size was increased.[15]

Very recently, $(BiO)_2CO_3$ as a new semiconductor photocatalytic material has received intensive research interests for its attractive morphology and multi-functional applications. Chen and co-workers prepared various of $(BiO)_2CO_3$ nanostructures via a simple reflux process.[16-17] Xie's group synthesized $(BiO)_2CO_3$ sponge, flower and plate like nanostructures.[18] $(BiO)_2CO_3$ nanosheets and flower-like structures were prepared by Huang *et al*.[19] Cao's group have fabricated persimmon-like $(BiO)_2CO_3$ by a template method.[20] Yu and co-workers synthesized $BiVO_4/(BiO)_2CO_3$ and grapheme/$(BiO)_2CO_3$ nanocomposites by the hydrothermal method.[21-22] Our research team fabricated N-doped $(BiO)_2CO_3$, Ag/$(BiO)_2CO_3$ and Bi/$(BiO)_2CO_3$ hierarchical microspheres by a one pot template-free method.[23-27] Given the low activity of pure $(BiO)_2CO_3$ with limited visible light absorption, it is highly desirable to develop alternative approaches to enhance the photocatalysis efficiency. To the best of our knowledge, size-controlled Au NPs deposited $(BiO)_2CO_3$ microspheres have never been reported.

In this study, we reported a series of Au/$(BiO)_2CO_3$ heterostructures (Au/BOC) with size-controlled Au NPs uniformly dispersed onto the surface of $(BiO)_2CO_3$ microspheres. The samples were used for visible light photocatalytic removal of NO in air. The results showed that the Au/BOC exhibited enhanced photocatalytic activity in comparison with pure $(BiO)_2CO_3$, which can be ascribed to the SPR effect and efficient separation of electron-hole pairs by Au NPs. Meanwhile, the effect of Au NPs content and size on the photocatalytic performance was evaluated. The sample loading with 2-4 nm Au NPs exhibited the highest photocatalytic activity. This work could provide new insights into the design and synthesis of novel size-controlled cocatalyst-decorated photocatalytic materials for environmental and energetic applications.

Experimental Section

Preparation of photocatalysts

Preparation of Au NPs: Au NPs were prepared according to Brust's two-phase reaction procedure with some minor modifications.[28-29] Briefly, the hydrogen tetrachloroaurate trihydrate ($HAuCl_4 \cdot 3H_2O$)

aqueous solution (0.03 M, 3 ml) was added to tetraoctylammonium bromide (TOAB) in toluene (0.5 M, 3.6 ml), and the mixture was vigorously stirred. After stirring the solution mixed with different amount of 1-dodecanethiol (DDT) (0.11 M) and 3-mercaptopropionic acid (MPA, 0.11 M, 0.82 ml) in toluene for 15 min at room temperature, a freshly prepared aqueous solution (0.44 M, 2.045 ml) of sodium borohydride ($NaBH_4$) was added into the vigorously stirred solution. The resultant solution immediately turned from orange to deep brown and continued to be stirred for 15 min. The organic phase (about 4.43 ml) was transferred into 30 ml ethanol, followed by 5-min stirring. Then the solution was centrifugated and redispersed into 9 ml toluene. Here, the adding of DDT would control the growth of Au NPs, leading to different size of Au NPs when the adding amount of DDT varied from 0.82 to 0.42, 0.082 ml, and the corresponding as-prepared Au NPs were marked by Au-1 (2-4 nm), Au-2 (4-6 nm) and Au-3 (8-10 nm).

Preparation of $(BiO)_2CO_3$ microspheres: Sodium carbonate (0.46 g) was first dissolved in 70 ml distilled water in a 100 ml autoclaved Teflon vessel and then stirred for 10 min. Afterwards, 1.6 g bismuth citrate was added to the solution, and the mixture was further stirred for 30 min to ensure that all reagents were dissolved. The resulting precursor suspension was heated at 160 ℃ for 24 h. After being cooled down, the precipitate was collected, centrifuged and washed with water and ethanol four times, dried at 60 ℃ for 12 h to obtain the final sample which was labeled as BOC.

Deposition of Au NPs on $(BiO)_2CO_3$ microspheres: To realize controlled attachment of Au onto $(BiO)_2CO_3$ microspheres, it is important to use MPA as a linker to bind Au and $(BiO)_2CO_3$ microspheres. Firstly, the $(BiO)_2CO_3$ microspheres (0.2 g) were completely dispersed in 60 ml toluene by ultrasound for 30 min. Then the as-prepared Au NPs were dissolved in 4 ml toluene. The Au NPs solution was added dropwise to the $(BiO)_2CO_3$ suspension, and the resulted suspension was stirred magnetically at room temperature for 1 h. Lastly, the product was centrifuged and washed with water and ethanol four times, dried at 60 ℃ for 12 h. A series of Au deposited $(BiO)_2CO_3$ microspheres labeled as Au/BOC-X (X= 2ml, 4ml and 8 ml, respectively) with different amount of Au NPs (Au-1) were obtained by adding desired amount of Au NPs solution in the reaction system. In order to investigate the influence of the size of Au NPs, the Au/BOC-X (X= 1, 2 and 3, respectively) were synthesized with the similar procedure by using 4 ml Au NPs solution. In the procedure, MPA serves as a linker to bind BOC and Au NPs (Scheme 1).[30-31]

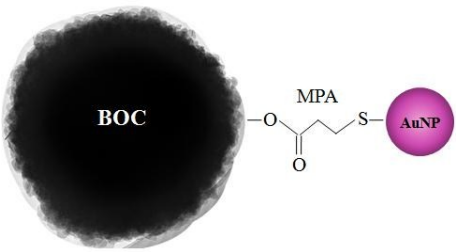

Scheme 1. Binding between BOC and Au NPs using MPA.

Characterization

The crystalline structure of the as-prepared samples were analyzed by an X-ray diffractometer (XRD, Model D/max RA, Rigaku Co., Japan), using Ni-filter Cu Kα radiation at 40 kV and 30 mA in the 2θ range from 5 to 80° with a scan rate of 4°/min. The morphology, structure and grain size of the obtained samples were characterized by transmission electron microscope (TEM, JEM-2010, Japan), and high-resolution transmission electron microscope (HRTEM). FT-IR spectra were recorded on a Nicolet Nexus spectrometer over the range of 400-4000 cm^{-1}. Surface chemical compositions and states were measured with an X-ray photoelectron spectroscope (XPS, Thermo ESCALAB 250, USA) equipped with Al Kα X-ray (hv = 1486.6 eV) radiation source. The Brunauer-Emmett-Teller (BET) measurements of specific surface area and pore size distribution of the samples were determined using a nitrogen adsorption apparatus (ASAP 2020, USA) with all samples degassed at 130 ℃ for 4h prior to measurements. The UV-vis diffuse reflection spectra (UV-vis DRS) were obtained for the dry-pressed disk samples by using a Scan UV-vis spectrophotometer (UV-2450, Shimadzu, Japan) with 100% $BaSO_4$ as the standard sample. A fluorescence spectrophotometer (PL, F-7000, Japan) was used to record PL spectra using Xe lamp with optical filters as the excitation source.

Evaluation of photocatalytic activity

The photocatalytic activity of the as-synthesized samples was evaluated by removing NO at ppb level in a continuous flow reactor with volume of 4.5 L (30 cm × 15 cm × 10 cm). The reactor was made of organic glass and covered with Saint-Glass. A 150 W commercial tungsten halogen lamp vertically located 20 cm above the reactor was used as the visible light source. For the visible light driven photocatalysis, a piece of UV cutoff glass was employed to remove all the UV light with the wavelength below 420 nm. The 0.2 g of photocatalyst sample was dispersed in 30 ml of distilled water in a beaker by ultrasonic treatment for 10 min, and then coated onto two glass dishes with a diameter of 12.0 cm. The dishes containing the photocatalyst were pretreated at 70°C until complete removal of water in the suspension and then placed in the center of the reactor after cooling down to room temperature. The NO gas was acquired from a compressed gas cylinder at a concentration of 100 ppm of NO (N_2 balance, BOC gas). The initial concentration of NO was diluted to about 600 ppb by the air stream supplied by an air cylinder. The flow rate of air stream and NO were controlled at 2.4 L min^{-1} and 15 mL min^{-1}, respectively. Then the two gas streams were premixed completely by a three-way valve. After reaching the adsorption-desorption equilibrium on the photocatalyst, the lamp was turned on to start the photocatalysis reaction. The concentration of NO, NO_2 and NO_x (NO_x represents NO + NO_2) were measured by a NO_x analyzer (Thermo Scientific, 42i-TL) every one min. The NO removal rate (η) was calculated by the following equation: η (%) = $(1 - C/C_0) \times 100\%$, where C and C_0 represent the NO concentration determined before and after reaction.

Results and discussion

Phase structure

Fig. 1 shows the XRD patterns of as-prepared $(BiO)_2CO_3$ and Au/BOC composites with different size and content of Au NPs. The diffraction peaks for all the samples can be indexed to tetragonal $(BiO)_2CO_3$ phase (JCPDS Card No. 41-1488). The addition of Au NPs with different sizes and amount has little influence on the phase structure of $(BiO)_2CO_3$. Note that there are no obvious diffraction peaks of Au, as the content of Au NPs is too low to be detected.[28]

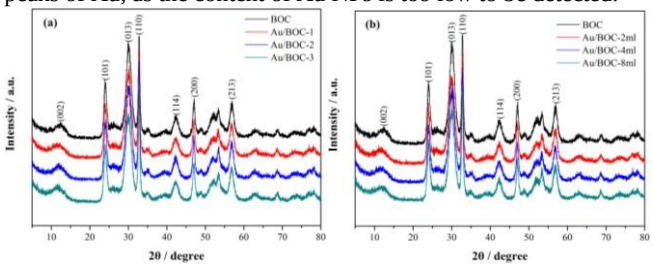

Fig. 1 XRD patterns of as-prepared BOC and Au/BOC composites.

Morphological structure

The morphological structure of the Au/BOC composites with different Au size is further investigated by TEM. Fig. 2a and 2b displays the TEM images of Au/BOC-1. The Au NPs are dispersed evenly on the $(BiO)_2CO_3$ microspheres as shown in Fig. S1 (ESI†). The HRTEM image reveals that the introduced Au NPs is about ~4 nm. When reducing the adding amount of DDT, the Au NPs grow larger, which is clearly in the Fig. 2c and 2e (Fig. S2 and Fig. S3, ESI†). The size of Au NPs in the samples of Au/BOC-2 and Au/BOC-3 are about ~6 nm and ~8 nm, respectively. From the HRTEM images, the lattice of Au NPs and $(BiO)_2CO_3$ can be clearly observed. The lattice spacing are determined to be 0.272 and 0.234 nm, matching the (110) plane of $(BiO)_2CO_3$ and (111) plane of Au, respectively. The morphological structures of the Au/BOC composites with different amount of Au-1 NPs are displayed in Fig. 3 and Fig. S4 (ESI†). When reduing the amount of Au-1 NPs to 2 ml, Au NPs are scarcely dispersed on $(BiO)_2CO_3$ support (Fig. 3a and 3b). When increasing the amout of Au-1 NPs to 8 ml, the Au coverage is too large that some are partially aggregated (Fig. 3c and 3d, Fig. S5, ESI†).

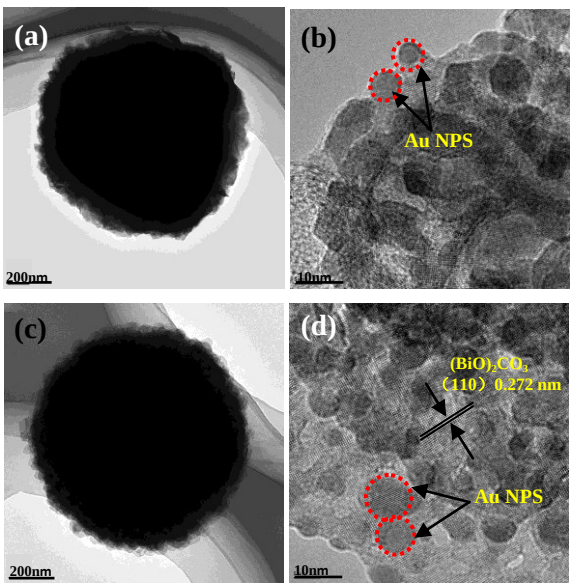

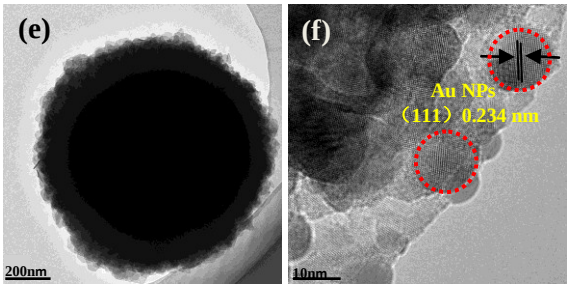

Fig. 2 TEM and HRTEM images of Au/BOC composites: (a, b) Au/BOC-1, (c, d) Au/BOC-2 and (e, f) Au/BOC-3. The adding amount of Au NPs was 4 ml.

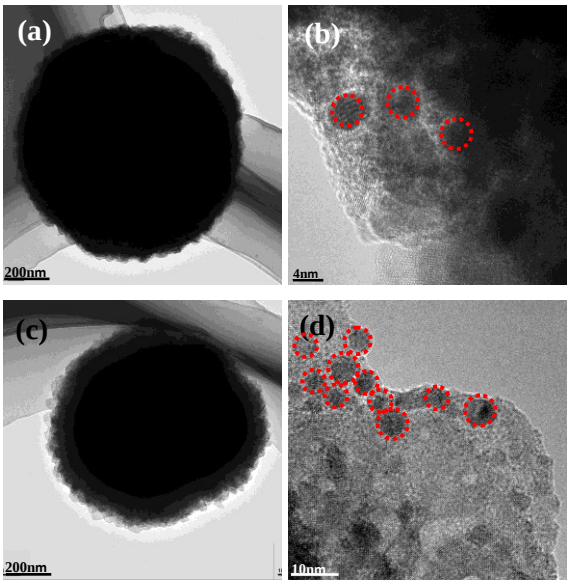

Fig. 3 TEM and HRTEM images of Au/BOC composites with different Au NPs content: (a, b) 2 ml and (c, d) 8 ml. The Au NPs size is controlled at 2-4nm.

Chemical composition

Fig. S6 (ESI†) represents the FT-IR spectra of the as-prepared samples. The broadband at 1580 cm^{-1} and 3500 cm^{-1} are believed to be associated with the stretching vibrations of surface hydroxyl groups and adsorbed water molecules.[24-25] The "free" CO_3^{2-} ions have four internal vibration forms: symmetric stretching mode v_1, anti-symmetric stretching mode v_3, out-of-plane bending mode v_2 and in-plane bending mode v_4. The bands located at 1067 and 846 cm^{-1} can be assigned to mode v_1 and mode v_2, respectively. While the peaks at 1468 and 1391 cm^{-1} can be ascribed to mode v_3. The mode v_4 can also be detected at 698 and 670 cm^{-1}. Additionally, the band found at 548 cm^{-1} can be attributed to the Bi-O stretching. Comparing the spectra of BOC and Au/BOC composites, we find that the bands at 548 and 846 cm^{-1} of Au/BOC composites become weaker, suggesting BOC is partly covered by Au NPs deposited on its surface, which can be observed from the TEM images.

The XPS technique was employed to analyze the surface composition of Au/BOC-8ml. Fig. S7a (ESI†) presents the high-resolution spectra of Bi4f. The binding energy peaks located at 158.7 and 164.1 eV are assigned to $Bi4f_{7/2}$ and $Bi4f_{5/2}$, respectively, which is the feature of Bi^{3+} in $(BiO)_2CO_3$.[32] As shown in Fig. S7b (ESI†), the C1s peak at binding energy of 284.77 eV is caused by the

adventitious carbon species, while the peak at 288.5 eV can be ascribed to the CO_3^{2-} in $(BiO)_2CO_3$. The O1s peak (Fig. S7c, ESI†) at 529.7 is characteristic of Bi-O in $(BiO)_2CO_3$. The other two peaks at 531.0 and 532.8 eV can be assigned to CO_3^{2-} and hydroxyl groups on the surface. Two peaks in Fig. S7d (ESI†) at 83.3 and 86.9 eV refer to $Au4f_{7/2}$ and $Au4f_{5/2}$, respectively, which are lower than those of metallic Au ($Au4f_{7/2}$, 84 eV; $Au4f_{5/2}$, 87.7 eV).[33] This finding can be ascribed to the strong interaction caused by MPA between Au NPs and BOC, leading to partial electron transfer from BOC to Au NPs.[34]

BET surface areas and pore structure

Fig. S8 (ESI†) exhibits the nitrogen adsorption-desorption isotherms and the corresponding pore size distribution curves of $(BiO)_2CO_3$ and Au/BOC composites. Typically, each of these samples has an isotherm of type IV (Fig. S8a and S8c, ESI†), indicating the presence of mesopores. The calculated BET surface areas are listed in Table S1 (ESI†). Clearly, the BET surface area of BOC sample is the highest (46 m^2/g). After the introduction of Au NPs, the BET areas are decreased slightly. The corresponding pore size distribution curves of the samples are shown in Fig. S8b and S8d (ESI†), and the corresponding pore volume data are listed in Table S1 (ESI†). For all these six samples, the pore size distribution located in three ranges. The first range with the peak at about 3.6 nm can be ascribed to the distribution of Au NPs on the $(BiO)_2CO_3$ microspheres. The second range with the peak at about 7.3 nm can be attributed to the pores formed among the self-assembled nanosheets of $(BiO)_2CO_3$ microspheres. And the third range with the peak at about 49.4 nm can be ascribed to the pores formed among the stacked $(BiO)_2CO_3$ microspheres.

UV-vis DRS and PL

The UV-vis DRS spectra of Au/BOC and pure $(BiO)_2CO_3$ samples are shown in Fig. 4. It's noteworthy to mention that there is a broad absorption in the visible light region from 500 to 700 nm for Au/BOC composites. Such absorption ability in the visible light region should be attributed to the SPR effect of metallic Au NPs.[35-36] However, the Au/BOC-2 and Au/BOC-3 samples do not exhibit obvious SPR absorption (Fig. 4a). For series of Au particle sizes, the mass of Au is identical. When the Au particles grow bigger, the number of Au particles would be decreased, which results in low SPR absorption of Au/BOC-2 and Au/BOC-3 with bigger Au sizes. The above results are in agreement with the TEM images. Fig. 4b reveals that the samples exhibit increased absorption in the visible light region with increasing Au content. The stronger SPR effect is caused by more deposited Au NPs, making Au/BOC absorb more solar light.[35-36] In general, the deposition of Au NPs could significantly enhance the visible light absorption of $(BiO)_2CO_3$ microspheres.

The electron-hole separation efficiency of the as-prepared samples was characterized by PL spectra, as shown in Fig. S9 (ESI†). The Au/BOC-8ml shows significantly diminished PL intensity compared with pure BOC, which suggests that the deposition of Au with MPA as the linker results in a remarkable decline in the recombination rate of electron–hole pairs.

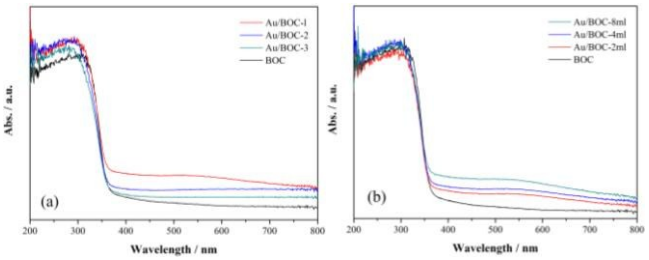

Fig. 4 UV-vis DRS spectra of BOC and Au/BOC composites.

Photocatalytic activity and mechanism

The photocatalytic activities of the obtained Au/BOC nanocomposites were evaluated in terms of NO removal in gas phase. Previous reports have demonstrated that no significant decrease in NO content is observed in the absence of either light irradiation or photocatalyst, suggesting that the NO oxidation is mainly driven by photocatalysis.[32] The main final product for photocatalytic NO removal is determined as NO_3^-.[25, 32] Fig. 5 shows the variation of NO concentration (C/C_0%) with irradiation time for Au/BOC samples under visible light irradiation with pure $(BiO)_2CO_3$ as references. Pure $(BiO)_2CO_3$ hierarchical microsphere exhibit decent visible light photocatalytic activity through surface scattering and reflecting (SSR) effect (Scheme 2).[37-38] It is obvious to observe that all of the Au/BOC samples exhibit higher photocatalytic activities for the NO removal compared with the pure $(BiO)_2CO_3$ (112 ppb/min), which is ascribed to the SPR effect and pronounced charge separation of Au/BOC. It is well known that the Au particle on semiconductor could effectively separate the photogenerated electron-hole pairs through schottky heterojunction.[39-40] In Au size-controlled sample series (Fig. 5a), the Au/BOC-1 shows the highest photocatalytic activity (203 ppb/min). As the size increases, the activity decreases to 177 ppb/min. The reason for the low activity of the larger particle sizes can be identified from their UV-Vis spectra and specific surface area. The light absorption by the sample loaded with larger Au NPs is negligible (Fig. 4a), indicating a weaker SPR effect.[41] The light absorption is important for the photocatalytic performance, but the performance also depends on other factors, particularly the specific surface areas of the Au NPs. Smaller Au NPs have a larger specific surface area and generally possess a larger number of active sites. The relative large surface area and stronger SPR absorption could contribute to a higher catalytic conversion.

In the Au concentration series samples (Fig. 5b), the photocatalytic NO conversion increases from 180 to 203 ppb/min with increasing Au content from 2 ml to 4 ml. However, further increasing the amount of Au NPs to 8 ml leads to a decrease in photocatalytic conversion (191 ppb/min), which can be ascribed to the partially aggregation and excess amount of Au NPs (Fig. 3d). The aggregated Au NPs are not favorable for SPR effect. It's well known that depositing a certain amount of noble metal on the surface of a photocatalyst might improve the migration efficiency of photogenerated electrons and suppress the recombination of hole-electron pairs effectively. While over abundance of noble metal would become the recombination centers of electrons and holes, and finally resulting in the decrease of activity.[42-43] The result indicates that an deposition of appropriate amount of metallic Au with suitable

particle size could significantly enhance the visible light photocatalytic activity of $(BiO)_2CO_3$ microspheres.

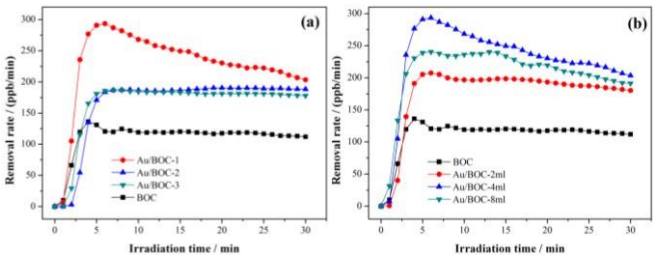

Fig. 5 Visible light photocatalytic activity of Au/BOC and BOC samples for the removal of NO.

As elucidated in Scheme 2, the enhanced photocatalytic activity of Au/BOC can be attributed to the synergetic effects of the following factors. Firstly, the SPR effect of Au NPs propels the Au/BOC samples to absorb more visible light. Also, owing to the SPR effect, the Au NPs can be photoexcited, thus enhancing the surface electron excitation and interfacial electron transfer.[44] Second, since the Fermi level of Au (0.45 eV) is lower than the CB of $(BiO)_2CO_3$ (0.20 eV), the photogenerated electrons would probably transfer from $(BiO)_2CO_3$ to Au NPs, creating a Schottky barrier at the interface that reduces the recombination of electron-hole pairs.[45]

According to our previous investigation, the $(BiO)_2CO_3$ microspheres exhibited enhanced extrinsic absorption benefiting from the strong light scattering and reflecting effects (SSR).[37-38] Due to the presence of defects, the SSR effect can induce the production of electron-hole pairs.[37-38] After the separation of electrons and holes, these two kinds of photogenerated charge carriers would be transformed into active species (•OH) that are responsible for the degradation of NO. As the redox potential of O_2/H_2O_2 is 0.695 eV, the photoexcited electrons of Au together with the electrons transferred from $(BiO)_2CO_3$ can reduce O_2 to H_2O_2. The formed H_2O_2 would be further transformed into •OH by capturing an electron.[46] Meanwhile, the potential of the holes at the VB of $(BiO)_2CO_3$ (3.53 eV) is more positive than the redox potential of $OH^-/•OH$ (1.99 eV), and therefore the holes can oxidize OH^- to •OH. The •OH radicals as major reactive oxidation species could oxidize NO to final NO_2^- and NO_3^- product.[47,48]

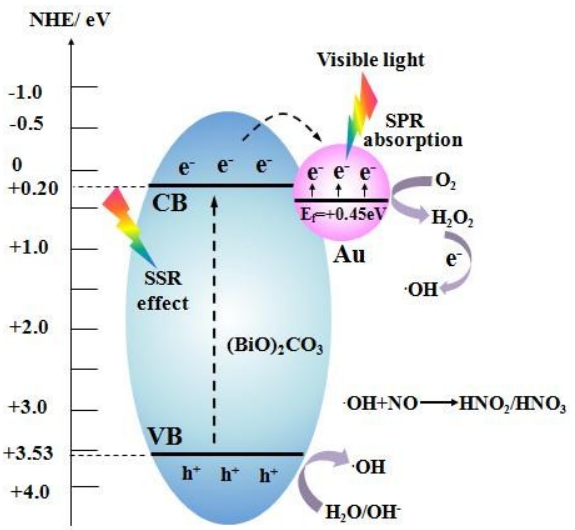

Scheme 2. Photocatalytic mechanism of Au/BOC under visible light irradiation.

Conclusions

In summary, we have developed a novel Au/BOC heterostructure with size-controlled Au NPs uniformly dispersed onto the surface of $(BiO)_2CO_3$ microspheres. The Au and $(BiO)_2CO_3$ microspheres were linked by MPA. The enhanced visible light photocatalytic activity of Au/BOC samples can be ascribed to the cooperative contribution of SPR effect and efficient separation of electron-hole pairs by Au NPs. Among the Au size-controlled series, the Au/BOC-1 sample with small Au particle size exhibited the most efficient visible light photocatalytic activity, which can be attributed to its stronger visible light absorption and smaller NPs that could provide more active sites. For Au content-controlled series, the Au/BOC-4ml with appropriate Au loading exhibited the highest photocatalytic activity. Loading appropriate amount of Au NPs with small size could significantly enhance the visible light photocatalytic activity of $(BiO)_2CO_3$ microspheres. We have also proposed a new photocatalysis mechanism involved with SSR coupled with SPR. This work could provide new insights into the fabrication and understanding of size-controlled metal/semiconductor photocatalytic materials for environmental pollution control and solar energy conversion.

Acknowledgement

This research is financially supported by the National Natural Science Foundation of China (51478070, 51108487) and Postgraduate Innovation Research Project of Chongqing Technology and Business University (yjscxx2014-052-28).

Notes and references

[a]*Chongqing Key Laboratory of Catalysis and Functional Organic Molecules, College of Environmental and Biological Engineering, Chongqing Technology and Business University, Chongqing 400067, P. R. China. E-mail: dfctbu@126.com*

[b]*College of Materials Science and Engineering, Chongqing University, Chongqing 400044, P. R. China. E-mail: zhangyuxin@cqu.edu.cn*

[c]*National Key Laboratory of Fundamental Science of Micro/Nano-Devices and System Technology, Chongqing University, Chongqing 400044, P. R. China.*

† Electronic supplementary information (ESI) available. See DOI:10.1039/

‡ Qiuyan Li and Xiaodong Hao contributed equally to this work.

1 X. B. Chen and S. S. Mao, *Chem. Rev.*, 2007, **107**, 2891.
2 M. Ye, J. Gong, Y. Lai, C. Lin and Z. Lin, *J. Am. Chem. Soc.*, 2012, **134**, 15720.
3 H. Park, Y. K. Kim and W. Choi, *J. Phys. Chem. C*, 2011, **115**, 6141.
4 M. Jakob, H. Levanon and P. V. Kamat, *Nano. Lett.*, 2003, **3**, 353.
5 A. Takai and P. V. Kamat, *ACS. Nano.*, 2011, **5**, 7369.
6 V. Subramanian, E. E. Wolf and P. V. Kamat, *J. Am. Chem. Soc.*, 2004, **126**, 4943.
7 P. D. Cozzoli, M. L. Curri and A. Agostiano, *Chem. Commun.*, 2005, 3186.

8 S. Linic, P. Christopher and D. B. Ingram, *Nature. Mater.*, 2011, **10**, 911.
9 S. K. Cushing, J. T. Li, F. Meng, T. R. Senty, S. Suri, M. J. Zhi, M. Li, A. D. Bristow and N. Q. Wu, *J. Am. Chem. Soc.*, 2012, **134**, 15033.
10 P. Wang, B. B. Huang, Y. Dai and M. H. Whangbo, *Phys. Chem. Chem. Phys.*, 2012, **14**, 9813.
11 M. M. Alvarez, J. T. Khoury, T. G. Schaaff, M. N. Shafigullin, I. Vezmar and R. L. Whetten, *J. Phys. Chem. B*, 1997, **101**, 3706.
12 R. C. Jin, Y. W. Cao, C. A. Mirkin, K. L. Kelly, G. C. Schatz and J. G. Zheng, *Science.*, 2001, **294**, 1901.
13 A. T. Bell, *Science.*, 2003, **299**, 1688.
14 A. Janz, A. K çkritz, L. Yao and A. Martin, *Langmuir.*, 2010, **26**, 6783.
15 X. Chen, H. Y. Zhu, J. C. Zhao, Z. F. Zheng and X. P. Gao, *Angew. Chem. Int. Ed.*, 2008, **47**, 5353.
16 R. Chen, M. H. So, J. Yang, F. Deng and H. Z. Sun, *Chem. Commun.*, 2006, 2265.
17 G. Cheng, H. M. Yang, K. F. Rong, Z. Lu, X. L. Yu and R. Chen, *J. Solid. State. Chem.*, 2010, **183**, 1878.
18 Y. Zheng, F. Duan, M. Q. Chen and Y. Xie, *J. Mol. Catal. A*, 2010, **317**, 34.
19 Y. Y. Liu, Z. Y. Wang, B. B. Huang, K. S. Yang, X. Y. Zhang, X. Y. Qin and Y. Dai, *Appl. Surf. Sci.*, 2010, **257**, 172.
20 X. F. Cao, L. Zhang, X. T. Chen and Z. L. Xue, *CrystEngComm.*, 2011, **13**, 1939.
21 P. Madhusudan, J. R. Ran, J. Zhang, J. G. Yu and G. Liu, *Appl. Catal. B*, 2011, **110**, 286.
22 P. Madhusudan, J. G. Yu, W. G. Wang, B. Cheng and G. Liu, *Dalton. Trans.*, 2012, **41**, 14345.
23 F. Dong, W. K. Ho, S. C. Lee, Z. B. Wu, M. Fu, S. C. Zou and Y. Huang, *J. Mater. Chem.*, 2011, **21**, 12428.
24 F. Dong, S. C. Lee, Z. B. Wu, Y. Huang, M. Fu, W. K. Ho, S. C. Zou and B. Wang, *J. Hazard. Mater.*, 2011, **195**, 346.
25 F. Dong, Y. J. Sun, M. Fu, W. K. Ho, S. C. Lee and Z. B. Wu, *Langmuir.*, 2012, **28**, 766.
26 F. Dong, H. T. Liu, W. K. Ho, M. Fu and Z. B. Wu, *Chem. Eng. J.*, 2013, **214**, 198.
27 F. Dong, Q. Y. Li, Y. J. Sun and W. K. Ho, *ACS Catal.*, 2014, **4**, 4341.
28 Y. X. Zhang and H. C. Zeng, *J. Phys. Chem. B*, 2006, **110**, 16812.
29 M. Brust, M. Walker, D. Bethell, D. J. Scjoffrin and R. Whyman, *J. Chem. Soc. Chem. Commun.*, 1994, 801.
30 Y. X. Zhang, M. Huang, X. D. Hao, M. Dong, X. L. Li and J. M. Huang, *Nanoscale. Res. Lett.*, 2012, **7**, 295.
31 J. Li and H. C. Zeng, *Chem. Mater.*, 2006, **18**, 4270.
32 Z. H. Ai, W. K. Ho, S. C. Lee and L. Z. Zhang, *Environ. Sci. Technol.*, 2009, **43**, 4143.
33 D. A. Bulushev, I. Yuranov, E. I. Suvorova, P. A. Buffat and L. Kiwi-Minsker, *J. Catal.*, 2004, **224**, 8.
34 H. X. Li, Z. F. Bian, J. Zhu, D. Q. Zhang, G. S. Li, Y. N. Huo, H. Li and Y. F. Lu, *J. Am. Chem. Soc.*, 2007, **129**, 8406.
35 A. P. Zhang and J. Z. Zhang, *Appl. Surf. Sci.*, 2010, **256**, 3224.
36 H. Y. Li, W. B. Lu, J. Q. Tian, Y. L. Luo, A. M. Asiri, A. O. Al-Youbi and X. P. Sun, *Chem. Eur. J.*, 2012, **18**, 8508.
37 F. Dong, Q. Y. Li, Y. Zhou, Y. J. Sun, H. D. Zhang and Z. B. Wu, *Dalton. Trans.*, 2014, **43**, 9468.
38 T. Xiong, F. Dong and Z. B. Wu, *RSC. Adv.*, 2014, **4**, 56307.
39 Y. J. Luo, X. M. Liu, X. H. Tang, Y. Luo, Q. Y. Zeng, X. L. Deng, S. L. Ding and Y. Q. Sun, *J. Mater. Chem. A*, 2014, **2**, 14927.
40 G. Caria, M. Birsanu, K. Okada and H. Garcia, *J. Mater. Chem. A*, 2013, **1**, 9092.
41 P. Mulvaney, *Langmuir.*, 1996, **12**, 788.
42 J. Ren, W. Z. Wang, S. M. Sun, L. Zhang and J. Chang, *Appl. Catal. B*, 2009, **92**, 50.
43 C. Young, T. M. Lim, K. Chiang, J. Scott and R. Amal, *Appl. Catal. B*, 2008, **78**, 1.
44 M. J. Kale, T. Avanesian and P. Christopher, *ACS Catal.*, 2014, **4**, 116.
45 S. J. Peng, P. N. Zhu, S. G. Mhaisalkar and S. Ramakrishna, *J. Phys. Chem. C*, 2012, **116**, 13849.
46 Q. J. Xiang, J. G. Yu, B. Cheng and H. C. Ong, *Chem. Asian. J.*, 2010, **5**, 1466.
47 F. Dong, Z.W. Zhao, T. Xiong, Z.L. Ni, W.D. Zhang, Y.J. Sun and W.K. Ho, *ACS Appl. Mater. Interfaces.*, 2013, **5**, 11392.
48 F. Dong, Z. Wang, Y. Li, W. Ho, S. Lee, *Environ. Sci. Technol.*, 2014, **48**, 10345.

